



ELSEVIER

Available online at www.sciencedirect.com

SCIENCE @ DIRECT®

Journal of Contaminant Hydrology 81 (2005) 63–88

JOURNAL OF

Contaminant
Hydrology

www.elsevier.com/locate/jconhyd

Impact of rainfall intensity on the transport of two herbicides in undisturbed grassed filter strip soil cores

V. Pot^{a,*}, J. Šimůnek^b, P. Benoit^a, Y. Coquet^a,
A. Yra^{a,c}, M.-J. Martínez-Cordón^{a,d}

^a UMR INRA-INA P-G, Unité Environnement et Grandes Cultures, BP01, 78850 Thiverval-Grignon, France

^b Department of Environmental Sciences, University of California, Riverside, California, USA

^c UMR CNRS 8508-Laboratoire Transferts Ecoulements Fluides Energétiques, site de l'ENSAM, 33405 Talence Cedex, France

^d Departamento de Química Agrícola y Edafología, Campus Universitario de Rabanales, 14071 Córdoba, Spain

Received 9 July 2004; received in revised form 13 June 2005; accepted 19 June 2005

Available online 16 September 2005

Abstract

Two series of displacement experiments with isoproturon and metribuzin herbicides were performed on two undisturbed grassed filter strip soil cores, under unsaturated steady-state flow conditions. Several rainfall intensities (0.070, 0.147, 0.161, 0.308 and 0.326 cm h⁻¹) were used. A water tracer (bromide) was simultaneously injected in each displacement experiment. A descriptive analysis of experimental breakthrough curves of bromide and herbicides combined with a modeling analysis showed an impact of rainfall intensity on the solute transport. Two contrasting physical non-equilibrium transport processes occurred. Multiple (three) porosity domains contributed to flow at the highest rainfall intensities, including preferential flow through macropore pathways. Macropores were not active any longer at intermediate and lowest velocities, and the observed preferential transport was described using dual-porosity-type models with a zero or low flow in the matrix domain. Chemical non-equilibrium transport of herbicides was found at all rainfall intensities. Significantly higher estimated values of degradation rate parameters as compared to batch data were correlated with the degree of non-equilibrium sorption. Experimental breakthrough curves were analyzed using different physical and chemical equilibrium and non-equilibrium transport models:

* Corresponding author. Tel.: +33 1 30 81 54 02; fax: +33 1 30 81 53 96.

E-mail address: vpot@grignon.inra.fr (V. Pot).

convective–dispersive model (CDE), dual-porosity model (MIM), dual-permeability model (DP), triple-porosity, dual permeability model (DP-MIM); each combined with both chemical instantaneous and kinetic sorption.

© 2005 Elsevier B.V. All rights reserved.

Keywords: Pesticide transport; Nonequilibrium transport; Undisturbed soil columns; Breakthrough curves; Numerical model; HYDRUS-1D

1. Introduction

Grassed buffer strips were introduced as one of the best management practices to reduce soil losses due to erosion of cultivated soils. Located downslope of cropped fields and adjacent to streams or drainage ditches, grassed buffer strips are effective sediment traps and, moreover, have been shown to effectively remove soluble and sediment-bound chemicals from cropland runoff (Dillaha et al., 1989; Arora et al., 1996). Reviewing published data, Baker et al. (1995) found that herbicide runoff was reduced by an average of 48% by different types of buffer systems with reductions ranging from 9% to 91%. Many parameters such as soil type, soil water content, runoff volume, buffer width, and buffer vegetation can explain this variability (Patty et al., 1997). Vertical infiltration through the grass is the major reduction mechanism (Mersie et al., 1999). Physical filtration by the grass and sedimentation of the particle-bound pesticides at the soil surface further reduce the pesticide concentration in runoff water. The high potential for sorption and mineralization of pesticides in surface layers of the grassed soil has been pointed out in different studies (Hurto et al., 1979; Benoit et al., 1999). It is related to the high organic matter content of the topsoil, originating from the high biological activity in grassland soils (Merckx et al., 1985; Haynes and Francis, 1993). On the other hand, root growth and earthworm activity can lead to development of preferential pathways for soluble and sediment-bound pesticides that will then by-pass the surface horizon where pesticides can be retained and degraded. Therefore, there is a potential risk of pesticide contamination of shallow groundwater under grassed buffer strips. Field studies have reported preferential transport of herbicides through grassed buffer strips (Kanchanasut and Scotter, 1982; Delphin and Chapot, 2001). Runoff simulations performed at the local scale (i.e. 3 m²) and tension infiltrometer measurements at a smaller scale (50 cm²) showed the importance of infiltration in the reduction of pesticide runoff, but could not identify the particular mechanisms involved within the soil. Lateral sub-surface flow or vertical preferential transport through macropores were possible explanations (Souiller et al., 2002).

Although the high sorption capacities and mineralization rates in the grassed strips are well documented, the fate of pesticides inside the grassed buffer strip is still poorly understood. Especially, the role of infiltration needs to be better quantified. Some studies about vertical infiltration of pesticides in grassed buffer strip soils have been performed in the laboratory, using column displacement experiments. Mersie et al. (1999) showed that switchgrass roots caused preferential movement of bromide and atrazine herbicide in repacked soil columns. Reungsang et al. (2001) observed preferential transport of bromide and atrazine in undisturbed soil columns, although they found little difference in transport

characteristics between the switchgrass and adjacent cultivated soils. Other authors found contrasting results. Vogeler et al. (1997) did not observe preferential flow of anions in undisturbed soil columns sampled under pasture. Benoit et al. (2000) showed using undisturbed soil columns that leaching of isoproturon herbicide was significantly higher in the adjacent cropped soil compared to the grassed soil. They measured an enhanced isoproturon degradation due to the formation of nonextractable (bound) residues in the grassed soil. Leaching also depended on isoproturon aging in the soil before percolation in the columns.

This study focuses on the identification of the main flow and transport mechanisms in a grassed buffer strip soil and on the fate of two herbicides, isoproturon and metribuzin. A series of displacement experiments was performed at increasing rainfall intensities on two undisturbed soil columns, sampled from the topsoil of a grassed buffer strip. The modified one-dimensional transport model HYDRUS-1D (Šimůnek et al., 1998, 2003) was used to identify and quantify different physical and chemical non-equilibrium transport processes acting in the grassed soil.

2. Material and methods

2.1. Experimental

2.1.1. Soil description and core sampling

The studied grassed buffer strip is located at the experimental site of ARVALIS at La Jaillière in the western part of France (Loire-Atlantique). The 20-m-wide grassed strip, planted with perennial rye-grass (*Lolium perenne*) in 1992, is cut twice a year. The soil is a hydromorphic silt loam (24% clay, 40% silt, 36% sand) developed on altered schists of the Massif Armoricain. A perched aquifer often forms during the winter period at a depth of 25–60 cm and can occasionally reach the soil surface (Patty, 1997).

Two undisturbed soil cores (14-cm i.d. and 30-cm height) were sampled in June 2002 from the soil surface layer. To minimize soil compaction, a hydraulic pressure device was used to extract the cores. Bulk densities were sampled in the immediate vicinity. The arithmetic mean of the bulk density over the 0–30 cm depth was 1.25 g cm^{-3} .

2.1.2. Displacement experiments

Displacement experiments were conducted at steady-state flow under unsaturated conditions.

A CaCl_2 solution ($5.10^{-3} \text{ M CaCl}_2$) was supplied to the soil surface using a rainfall simulator consisting of 47 hypodermic needles (0.3-mm i.d.) at a 25-mm spacing. A membrane pump delivered a constant flux to the rainfall simulator. A stainless steel mesh (25 μm porosity) was placed at the soil base and covered with glass beads (95–150 μm diameter) to establish a full contact between the soil base and the mesh. To maintain unsaturated conditions, a negative pressure of -15 cm was applied at the mesh level by fixing the height between the base of the core and the constant water level outlet of the column apparatus. Two time domain reflectometry (TDR) probes (8-cm long uncoated mini-probes) were horizontally inserted 6 and 20 cm below the soil

surface to measure the volumetric water content inside the soil columns. Three tensiometers (2-cm long and 0.6-cm diameter) were located at 6, 15 and 25 cm below the soil surface to measure the soil water pressure head. The effluent was collected at fixed time intervals of 0.5 h at the highest velocity and 1.5 h at the intermediate and lowest velocities to obtain the breakthrough curves. Note that the length of the tubing below the base of the core was about 80 cm long and 4.8-mm i.d. The delay in the tubing was taken into account when the experimental breakthrough curves were constructed by correcting the arrival time of the effluents.

The displacement experiments consisted of injecting a pulse of the CaCl_2 solution containing actual concentrations of $66.1 \pm 2.1 \text{ mg l}^{-1}$ Br, $7.6 \pm 1.5 \text{ mg l}^{-1}$ isoproturon (IPU) and $8.5 \pm 0.2 \text{ mg l}^{-1}$ metribuzin (Met). Three and two successive displacement experiments were performed at different rainfall intensities for columns I and II, respectively. The solute pulse duration was fixed so that an approximately equal mass of Br, IPU and Met was injected at each velocity. Differences in flow rates between the pulse solution application and the rainfall were less than 10% for all experiments. Between the successive solute pulses, the columns were thoroughly rinsed with the CaCl_2 solution for several days until no solutes were detected in the effluent.

2.1.3. Herbicides properties

Isoproturon and metribuzin were purchased from CIL Cluzeau (France). Water solubilities for IPU and Met are 70 and 1200 mg l^{-1} ; K_{oc} values range from 36 to 241 l kg^{-1} and from 9 to 95 l kg^{-1} , and DT50s (half-lives) range from 12 to 33 days and from 23 to 180 days, respectively (Agritox, 2001). Met therefore shows higher mobility and persistence in soils than IPU. Madrigal et al. (2002) measured the sorption properties of IPU in the first 60-cm of the grassed strip at La Jaillière. The distribution coefficient, K_d , showed a strong vertical gradient (decreasing with the soil depth) that was correlated with the gradient of organic matter (also decreasing with the soil depth). Sorption and degradation properties were also measured by Benoit et al. (1999) in the same grassed strip. For IPU, a mean distribution coefficient was found to be equal to 2.4 l kg^{-1} , a mean K_{oc} 143 l kg^{-1} , a mean degradation rate 0.001203 h^{-1} , and a mean DT50 24 days, when considering the 0–30 cm horizon as one single layer.

2.1.4. Chemical analysis

Effluent was filtered on polyvinylidene difluoride syringe filters (0.45 μm) and stored at 4 °C until analysis. Bromide and herbicide concentrations were measured using a high performance liquid chromatography (Waters HPLC appliance) with an Allsep A-2 anion column for Br and a Nova Pack silica-C18 column (Waters) for IPU and Met. UV detection (Waters 996 Photodiode Array Detector) was performed at 194, 240 and 298 nm for Br, IPU and Met, respectively. Detection limits were 1 mg l^{-1} for Br and 0.001 to 0.01 mg l^{-1} for the herbicides.

2.2. Transport models

We used the HYDRUS-1D model that simulates water flow and transport of conservative and reactive solutes in soils (Šimůnek et al., 1998, 2003). The latest version

of the code implements different equilibrium and non-equilibrium flow and transport models in both direct and inverse mode. The following transport processes can be used to analyze experimental breakthrough curves (BTCs): a) physical and chemical equilibrium transport described using the classical convection–dispersion transport model (Lapidus and Amundson, 1952); b) chemical non-equilibrium transport using the two-site chemical model (Cameron and Klute, 1977); c) physical non-equilibrium transport using the two region model (mobile and immobile water) (van Genuchten and Wierenga, 1976) and the dual-permeability model (Gerke and van Genuchten, 1993); and finally, e) simultaneous physical and chemical non-equilibrium transport using the dual-permeability model (Gerke and van Genuchten, 1993) combined with the two-site chemical model.

Although we describe below only models that use the linear sorption isotherm, HYDRUS-1D can also consider nonlinear sorption using Freundlich or Langmuir sorption isotherms. Similarly, HYDRUS-1D considers transient flow and transport processes (Šimůnek et al., 2001), while below we describe only models for steady-state water flow condition.

2.2.1. Equilibrium transport model — CDE

Assuming that decay is active only in the liquid phase (assumed in all models described below) and linear relationship between liquid and solid phase concentrations: $s = K_d c$, where c (ML^{-3}) and s (MM^{-1}) are concentrations in the liquid and solid phases, respectively, and K_d is an empirical distribution constant (L^3M^{-1}), the transport of a reactive solute for steady-state water flow conditions can be written as follows:

$$\theta R \frac{\partial c}{\partial t} = \theta D \frac{\partial^2 c}{\partial z^2} - q \frac{\partial c}{\partial z} - \mu_w \theta c \quad (1)$$

where θ is the volumetric water content (L^3L^{-3}), D is the dispersion coefficient (L^2T^{-1}), q is the Darcian water flux (LT^{-1}), μ_w is first-order degradation constant for the solute in the liquid phase (T^{-1}), t (T) and z (L) are the temporal and spatial coordinates, respectively, and R is the retardation factor (–):

$$R = 1 + \frac{\rho K_d}{\theta} \quad (2)$$

where ρ is the bulk density (ML^{-3}).

2.2.2. Chemical non-equilibrium transport model

The concept of two-site sorption (Selim et al., 1977; van Genuchten and Wagenet, 1989) permits consideration of non-equilibrium adsorption–desorption reactions. The two-site sorption concept assumes that the sorption sites can be divided into two fractions: adsorbed concentration, s_e (MM^{-1}), is associated with one fraction of the sites (the type-1 sites) where sorption is assumed to be instantaneous, while adsorbed concentration, s_k (MM^{-1}), is associated with the remaining (type-2) sites where sorption is considered to be

a time-dependent, first-order kinetic process. The governing convection–dispersion equation is then written as follows:

$$\theta R_e \frac{\partial c}{\partial t} = \theta D \frac{\partial^2 c}{\partial z^2} - q \frac{\partial c}{\partial z} - \mu_w \theta c - \rho \alpha_{ch} [(1 - f_e) K_d c - s_k] \quad (3)$$

where f_e is the fraction of exchange sites assumed to be in equilibrium with the solution phase (–), α_{ch} is the first-order mass transfer rate constant (T^{-1}) for chemical non-equilibrium and R_e is the retardation factor for the equilibrium phase (–):

$$R_e = 1 + \frac{\rho f_e K_d}{\theta}. \quad (4)$$

2.2.3. Physical non-equilibrium transport models

2.2.3.1. Dual-porosity (mobile–immobile water) model — MIM. The concept of two-region, dual-porosity type solute transport (van Genuchten and Wierenga, 1976) permits consideration of physical non-equilibrium transport (MIM model). The two-region concept assumes that the liquid phase can be partitioned into mobile (flowing), θ_m ($L^3 L^{-3}$), and immobile (stagnant), θ_{im} ($L^3 L^{-3}$), flow regions and that solute exchange between the two liquid regions can be modeled as a first-order process. The governing convection–dispersion equation is then written as follows:

$$\theta_m R_m \frac{\partial c_m}{\partial t} = \theta_m D_m \frac{\partial^2 c_m}{\partial z^2} - q \frac{\partial c_m}{\partial z} - \mu_w \theta_m c_m - \alpha_{ph} (c_m - c_{im}) \quad (5)$$

where the subscript m and im refer to mobile and immobile regions, respectively; α_{ph} is the mass transfer rate coefficient (T^{-1}) for physical non-equilibrium; and R_m is the retardation factor in the mobile zone (–):

$$R_m = 1 + \frac{\rho f_m K_d}{\theta_m} \quad (6)$$

where f_m is the fraction of sorption sites in contact with mobile region.

2.2.3.2. Dual-permeability model — DP. The dual-permeability (DP) model (Gerke and van Genuchten, 1993; Šimůnek et al., 2003) assumes that the porous medium is composed of two mobile flow regions, each with its own flow and transport properties. The two regions are often alternatively referred to as matrix and fracture regions, micropores and macropores, or intra- and inter-porosity. Contrary to the dual-porosity model, dual-permeability model assumes that flow can occur in both domains. The total water content and water flux density are then defined as follows:

$$\begin{aligned} \theta &= w_f \theta_f + (1 - w_f) \theta_{ma} \\ q &= w_f q_f + (1 - w_f) q_{ma} \end{aligned} \quad (7)$$

where θ_{ma} and θ_f are volumetric water contents in the two pore regions ($L^3 L^{-3}$), q_{ma} and q_f are corresponding water fluxes (LT^{-1}), subscripts ma and f refer to the matrix and

fracture regions, and w_f is the volumetric weighting factor (–) expressing the ratio of the fracture domain to total volume.

The governing convection–dispersion equations for the matrix and fracture regions are written as follows:

$$\theta_{\text{ma}} R_{\text{ma}} \frac{\partial c_{\text{ma}}}{\partial t} = \theta_{\text{ma}} D_{\text{ma}} \frac{\partial^2 c_{\text{ma}}}{\partial z^2} - q_{\text{ma}} \frac{\partial c_{\text{ma}}}{\partial z} - \mu_w \theta_{\text{ma}} c_{\text{ma}} + \frac{\Gamma_s}{1 - w_f} \quad (8)$$

$$\theta_f R_f \frac{\partial c_f}{\partial t} = \theta_f D_f \frac{\partial^2 c_f}{\partial z^2} - q_f \frac{\partial c_f}{\partial z} - \mu_w \theta_f c_f - \frac{\Gamma_s}{w_f} \quad (9)$$

where the retardation coefficients are written as:

$$R_{\text{ma}} = 1 + \frac{\rho K_d}{\theta_{\text{ma}}}$$

$$R_f = 1 + \frac{\rho K_d}{\theta_f}. \quad (10)$$

Although in general reaction coefficients may be different in the two regions, in the formulation above we assume that both reaction coefficients (K_d and μ_w) and bulk densities are the same in both regions.

The transfer rate, Γ_s , for solutes between the fracture and matrix regions ($\text{ML}^{-3} \text{T}^{-1}$) is usually given as the sum of diffusive and convective fluxes. For steady-state water flow condition convective fluxes are equal to zero and Γ_s can thus be written as (Gerke and van Genuchten, 1996):

$$\Gamma_s = \alpha_s (1 - w_f) (c_f - c_{\text{ma}}) \quad (11)$$

where α_s is the first-order solute mass transfer rate coefficient (T^{-1}) of the form:

$$\alpha_s = \frac{\beta}{a^2} D_a \quad (12)$$

in which D_a is an effective diffusion coefficient ($\text{L}^2 \text{T}^{-1}$), which represents the diffusion properties of the fracture–matrix interface as well as other parameters, β is a shape factor that depends on the geometry (the value of β ranges from 3 for rectangular slabs to 15 for spherical aggregates), and a is the characteristic length of the aggregate (L) (e.g. the radius of a spherical or solid cylindrical aggregate, or half the width of a rectangular aggregate). In the following, we assumed spherical aggregates ($\beta=15$) and $a=0.1$ cm as the characteristic length of the aggregate (Kay, 1990).

2.2.3.3. Dual-permeability mobile–immobile water model — DP-MIM. Dual-permeability mobile–immobile water model (DP-MIM) assumes that the liquid phase in the matrix region can be further partitioned into mobile (flowing), $\theta_{\text{m,ma}}$ ($\text{L}^3 \text{L}^{-3}$), and immobile (stagnant), $\theta_{\text{im,ma}}$ ($\text{L}^3 \text{L}^{-3}$), regions:

$$\theta_{\text{ma}} = \theta_{\text{m,ma}} + \theta_{\text{im,ma}} \quad (13)$$

where θ_{ma} is the volumetric water content of the matrix pore system (L^3L^{-3}). The governing convection–dispersion equation for transport in the matrix region (8) is then replaced with modified Eq. (5):

$$\theta_{m,ma}R_{m,ma}\frac{\partial c_{m,ma}}{\partial t} = \theta_{m,ma}D_{m,ma}\frac{\partial^2 c_{m,ma}}{\partial z^2} - q_{ma}\frac{\partial c_{m,ma}}{\partial z} - \mu_w\theta_{m,ma}c_{m,ma} + \frac{\Gamma_s}{1-w_f} - \alpha_{ma}(c_{m,ma} - c_{im,ma}) \quad (14)$$

where $c_{im,ma}$ and $c_{m,ma}$ are solute concentrations in the immobile and mobile zones of the matrix region (ML^{-3}), respectively; and α_{ma} is the mass transfer rate coefficient between mobile and immobile zones of the matrix region (T^{-1}). The solute exchange between the two liquid regions in the matrix is modeled as a first-order process, i.e.,

$$\theta_{im,ma}R_{im,ma}\frac{\partial c_{im,ma}}{\partial t} = \alpha_{ma}(c_{m,ma} - c_{im,ma}) - \mu_w\theta_{im,ma}c_{im,ma} \quad (15)$$

with retardation coefficients $R_{m,ma}$ and $R_{im,ma}$ for the mobile and immobile domains of the matrix zone, respectively, given as:

$$R_{m,ma} = 1 + \frac{\rho f_{m,ma}K_d}{\theta_{m,ma}}$$

$$R_{im,ma} = 1 + \frac{\rho(1-f_{m,ma})K_d}{\theta_{im,ma}} \quad (16)$$

where $f_{m,ma}$ is the fraction of sorption sites in contact with mobile region in the matrix.

2.2.4. Physical and chemical non-equilibrium model

Simultaneous physical and chemical non-equilibrium processes are implemented in HYDRUS-1D using the dual-permeability model (Gerke and van Genuchten, 1993; Šimůnek et al., 2003). The governing convection–dispersion equations for the two regions are written as follows:

$$\theta_{ma}R_{ma}\frac{\partial c_{ma}}{\partial t} = \theta_{ma}D_{ma}\frac{\partial^2 c_{ma}}{\partial z^2} - q_{ma}\frac{\partial c_{ma}}{\partial z} - \mu_w\theta_{ma}c_{ma} + \frac{\Gamma_s}{1-w_f} - \rho\alpha_{ch}[(1-f_{ma})K_dc_{ma} - s_{kma}] \quad (17)$$

$$\theta_f R_f \frac{\partial c_f}{\partial t} = \theta_f D_f \frac{\partial^2 c_f}{\partial z^2} - q_f \frac{\partial c_f}{\partial z} - \mu_w \theta_f c_f - \frac{\Gamma_s}{w_f} - \rho \alpha_{ch}[(1-f_f)K_d c_f - s_{kf}] \quad (18)$$

where the adsorbed concentrations, s_{kma} and s_{kf} are associated with the type-2 sites in the matrix and fracture domains, respectively; f_{ma} and f_f are fractions of exchange sites assumed to be in equilibrium with the solution phase (–) in the matrix and fracture

domains, respectively; and α_{ch} is again the first-order mass transfer rate constant [T^{-1}]. The retardation coefficients are written again as:

$$R_{ma} = 1 + \frac{\rho f_{ma} K_d}{\theta_{ma}}$$

$$R_f = 1 + \frac{\rho f_f K_d}{\theta_f} \tag{19}$$

Note that in all formulations above we assume that the bulk density, reaction (K_d and μ_w) and transfer (α) coefficients are the same in both regions. The dual permeability model, however, allows for different dispersivities in the two pore regions.

3. Results

3.1. Descriptive analysis

3.1.1. Flow

A satisfactory steady-state flux was obtained for all cases (Table 1). For column I, the mean water content, derived from TDR measurements, slightly decreased by nearly 2% as rainfall intensity decreased, while for column II water contents remained about the same for both fluxes. For both columns, the water content in the upper part of the column was always slightly higher compared to the lower part. Pressure head measurements showed

Table 1
Measured flow properties and leaching chemical parameters

	q (cm h^{-1})	θ ($\text{cm}^3 \text{ cm}^{-3}$)	T_0 (-)	Br			IPU			Met		
				M (%)	T_{\min} (-)	T_{peak} (-)	M (%)	T_{\min} (-)	T_{peak} (-)	M (%)	T_{\min} (-)	T_{peak} (-)
<i>Column I</i>												
q_{\max}	0.308 ± 0.016	0.3980 ± 0.0212	0.1548	82.6 ^a	0.03	0.10	50.4 ^b	0.03	0.10	75.9 ^b	0.03	0.10
						0.21			0.21			0.21
q_{mid}	0.147 ± 0.059	0.3865 ± 0.0276	0.1521	95.6	0.13	0.49	35.4 ^c	0.32	0.75	n.d.	n.d.	n.d.
q_{\min}	0.070 ± 0.018	0.3766 ± 0.0086	0.168	98.9	0.09	0.60	13.0 ^d	0.14	0.92	48.5 ^d	0.09	0.80
<i>Column II</i>												
q_{\max}	0.326 ± 0.007	0.3745 ± 0.0078	0.1741	81.6	0.05	0.20	67.5 ^c	0.06	0.23	75.8 ^c	0.05	0.23
						0.41			0.41			0.41
q_{mid}	0.161 ± 0.003	0.3750 ± 0.0092	0.1712	83.3 ^f	0.13	0.51	58.2 ^g	0.02	0.26	49.7 ^g	0.09	0.39

q is the Darcian water flux measured from the effluent weights, q_{\max} , q_{mid} and q_{\min} correspond to the highest, intermediate and lowest rainfall intensities, respectively, θ is the volumetric water content, T_0 is the pulse duration, M is mass recovery, T_{\min} is the time of the first appearance of the chemical in the effluent, and T_{peak} is the time when the maximum chemical concentration was reached in the effluent. T_0 , T_{\min} and T_{peak} are expressed in pore volumes. Note that at q_{\max} , the arrival times of two peaks are presented. Measured after 2.8^a, 10.5^b, 7.9^c, 5.3^d, 10.3^e, 4^f, and 6.6^g pore volumes. n.d. is not determined. Standard errors are given after the \pm sign.

also slightly higher pressure heads (between 0 and -5 cm) close to the soil surface, compared to the other two locations (pressure heads ranged from -5 to -15 cm). Observed moisture gradients can be partially explained by the pressure head distribution and by the vertical variability of the hydraulic conductivity in this soil. Souiller et al. (2002) showed using in situ infiltrometer measurements that the surface layer (0–5 cm) has a higher hydraulic conductivity compared to the underlying layer (a factor from 3 up to 25 was observed) and they hypothesized that the vertical infiltration capacity of the grassed strip for conditions close to saturation was controlled by the hydrodynamic properties of the underlying layer. The hypothesis of a solely gravitational flow in a homogeneous soil was therefore not fully achieved in our column displacement experiments. However, considering that the water content did not change much with depth (less than 2%) when the flux rate was increased, the hypothesis of a gravity-driven flow was used as a first approximation.

3.1.2. Bromide and herbicides BTCs

The BTCs are plotted as the measured relative concentration (ratio of the effluent concentration, c , to the influent concentration, c_0) versus the number of pore volumes eluted (flux-averaged volume of solution eluted, V , per the column pore volume, V_0) (Figs. 1–3). Due to chemical analysis problems, the metribuzin BTC was not available in the case of the intermediate velocity of column I. From now on, for the sake of simplicity, we will use the following notation for the effluent velocities: the highest, intermediate and lowest rainfall intensities are, respectively, q_{\max} , q_{mid} and q_{\min} as defined in Table 1. Since for all experiments we used approximately the same pulse duration, a qualitative comparison between particular BTCs can be easily made.

For both columns, the Br BTCs for the q_{\max} case were markedly shifted to the left, exhibited double fronts or peaks and a significant asymmetry with a long tailing elution curve compared to the other velocities (Fig. 1). Arrival times of the two peaks were notably different for the two columns: at 0.1 and 0.21 pore volumes for column I with a relative concentration of 0.04 and 0.22, respectively, and at 0.23 and 0.41 pore volumes for column II with a relative concentration of 0.17 and 0.14, respectively. At q_{mid} and q_{\min} , comparable peak positions of the BTCs were observed (Table 1). Early arrivals of the peaks at q_{\max} indicated that a rapid transport of the tracer caused by a possible by-pass of the main part of the soil porosity and the use of macropore pathways probably occurred in the grassed strip soil at the largest rainfall intensity. Visual observation of several large macropores made by earthworm activity (of about 3 to 5 mm in diameter) and numerous root channels at the bottom of the soil columns (Fig. 4) suggested potential candidates for macroporous pathways.

At q_{\max} , the two herbicides elution curves displayed identical peak positions as those for Br (Figs. 2ad and 3ac and Table 1). No delay originating from soil-herbicide sorption was thus observed. These results supported the observation that preferential flow through macropores dominated at this high rainfall intensity.

At q_{mid} and q_{\min} , the comparison of arrival times of the concentration peaks of IPU and Met showed a delay as compared to Br for column I (Figs. 2bc and 3b), while earlier concentration peak arrivals than Br were found for column II (Figs. 2e and 3d). Note that a non-zero IPU concentration was found in the first effluent for column II at q_{mid} .

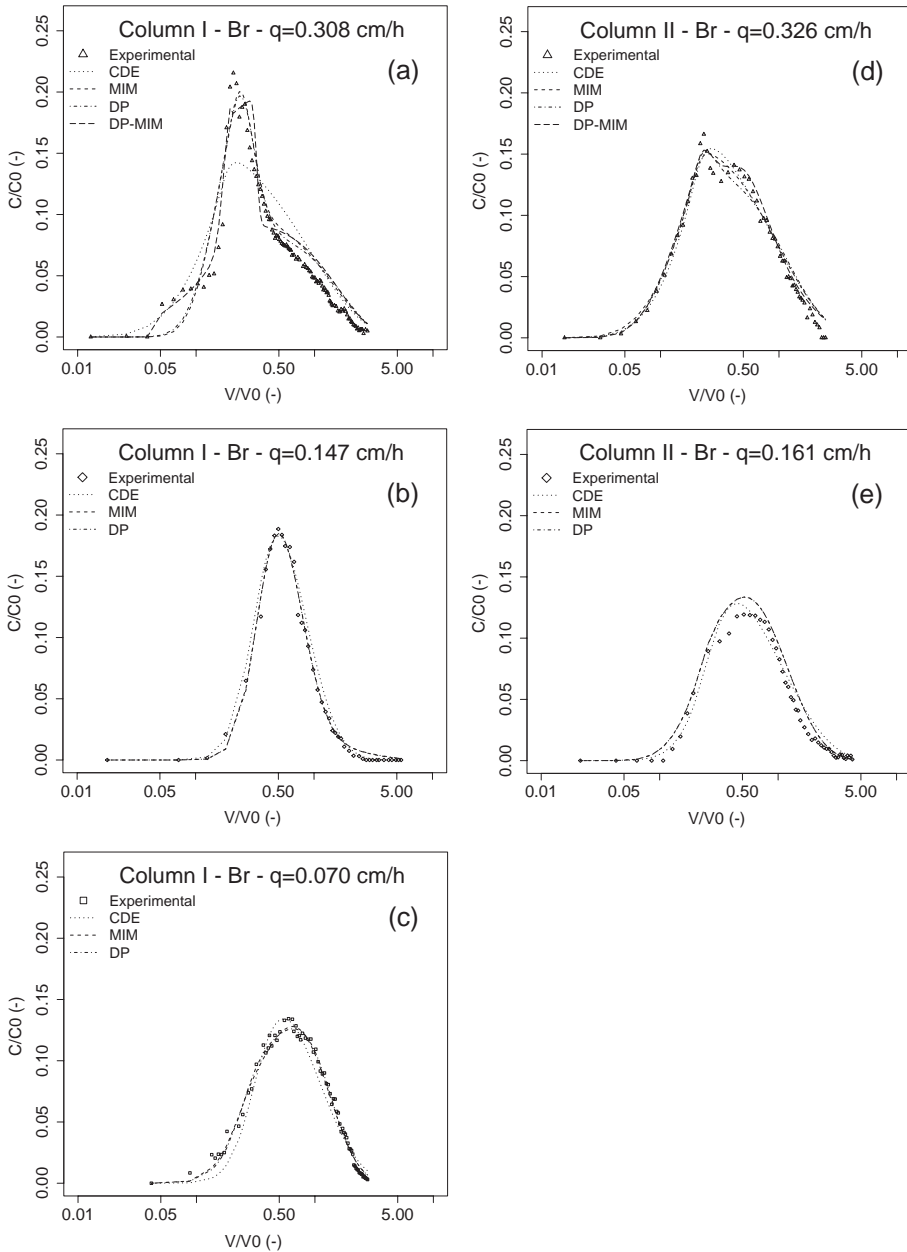


Fig. 1. Bromide BTCs measured and calculated for columns I and II using four different physical transport models. Symbols are the experimental data, dotted lines, dashed lines, dashed-and-dotted lines and long-dashed lines are the fits given by the CDE, MIM, DP and DP-MIM transport models, respectively. Relative concentrations of the effluents are presented against the number of pore volumes.

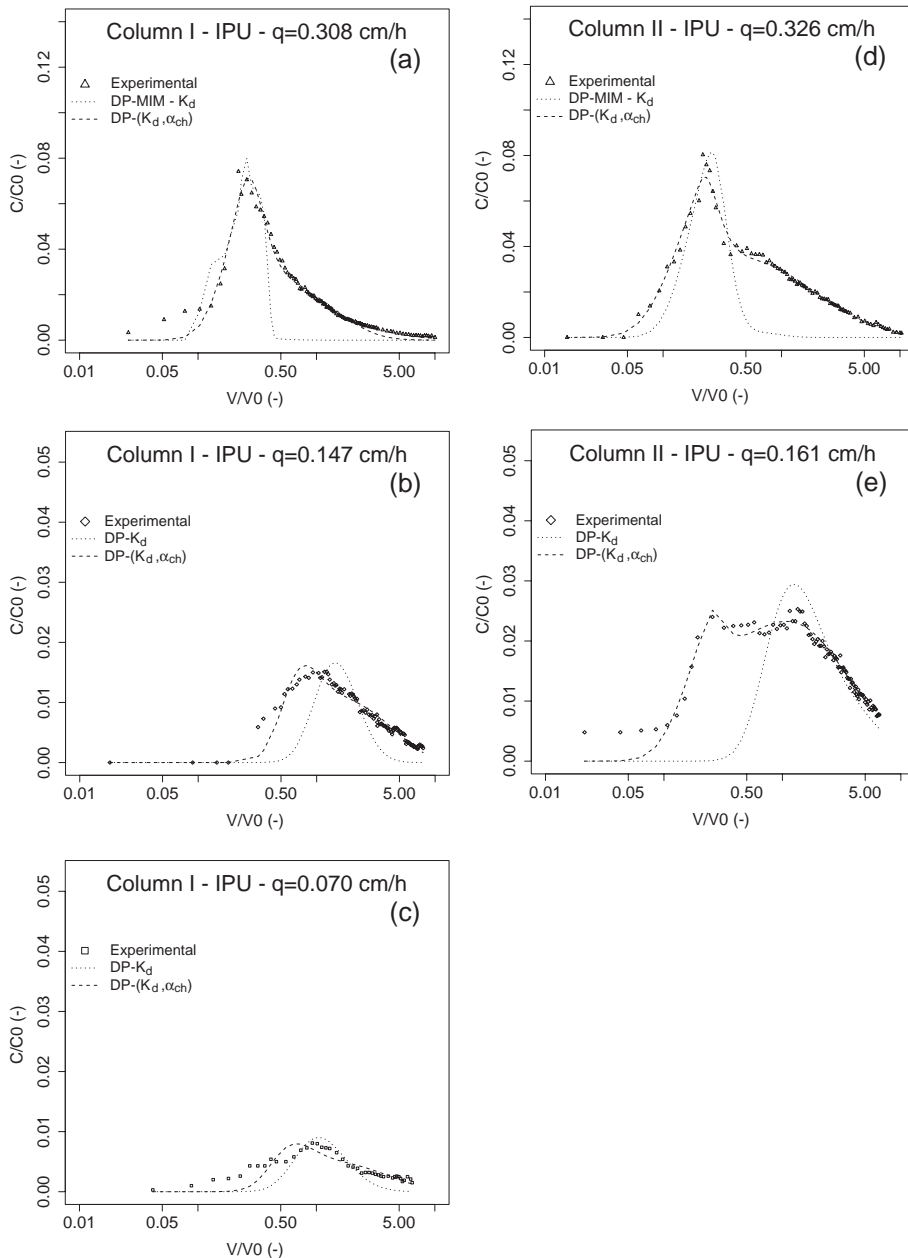


Fig. 2. Comparison of measured and calculated isotoproturon concentrations for columns I and II. The DP-MIM transport model was combined with the equilibrium chemical model (instantaneous sorption) for the highest rainfall intensities (DP-MIM- K_d transport model) and the DP transport model was combined with either the equilibrium (DP- K_d transport model) or non-equilibrium chemical models (instantaneous and first-order kinetic sorption) (DP-(K_d, α_{ch}) transport model) for the other rainfall intensities. Symbols represent the experimental data, dotted and dashed lines the DP-MIM- K_d or DP- K_d and DP-(K_d, α_{ch}) transport models, respectively. Relative concentrations of the effluents are presented against the number of pore volumes.

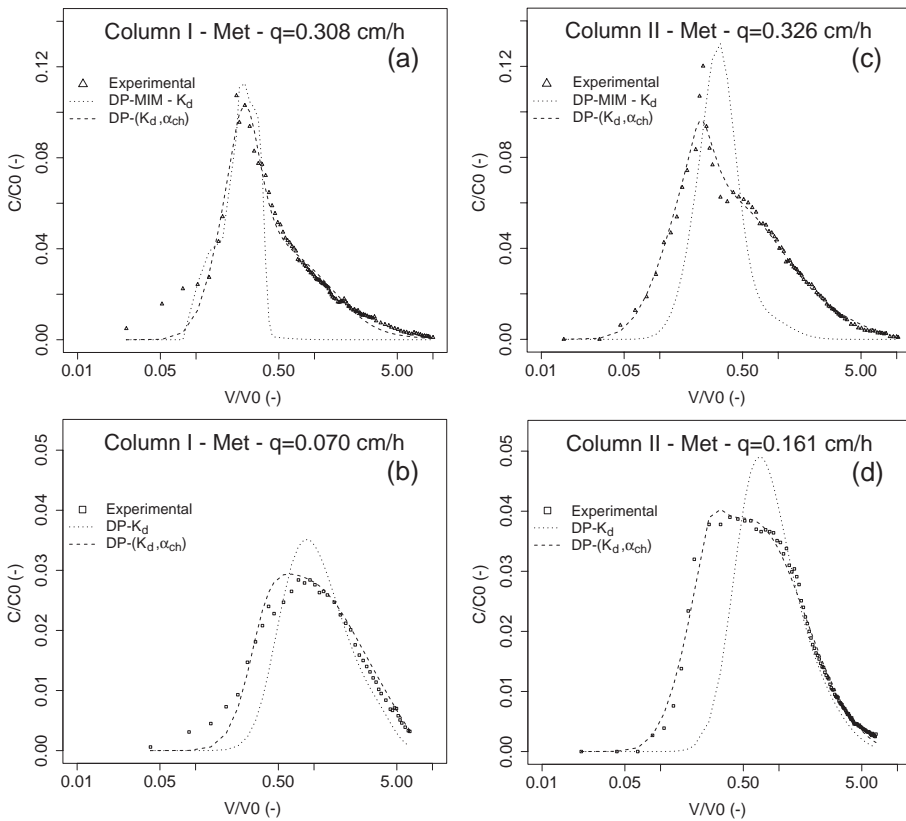


Fig. 3. Comparison of measured and calculated metribuzin concentrations for columns I and II. The DP-MIM transport model was combined with the equilibrium chemical model (instantaneous sorption) for the highest rainfall intensities (DP-MIM- K_d transport model) and the DP transport model was combined with either the equilibrium (DP- K_d transport model) or non-equilibrium chemical models (instantaneous and first-order kinetic sorption) (DP-(K_d, α_{ch}) transport model) for the other rainfall intensities. Symbols represent the experimental data, dotted and dashed lines the DP-MIM- K_d or DP- K_d and DP-(K_d, α_{ch}) transport models, respectively. Relative concentrations of the effluents are presented against the number of pore volumes.

For both herbicides, a decreasing mass recovery rate was found with decreasing velocity. This result was expected since the residence time of herbicides increased as velocity decreased and thus more time was left for sorption and degradation to occur inside the soil column. No degradation products were detected in the effluent. Since we had no experimental data about the fate of herbicides inside the soil columns, it was difficult to make conclusions about the potential decay processes in the soil column. Degradation with the formation of metabolites of lower mobility than the parent compound, mineralization, or irreversible sorption of either the parent compound or metabolites could have occurred in our soil columns. Benoit et al. (2000) showed in previous IPU percolation studies on the same grassed soil (i) the existence of metabolites in the soil, (ii) an increase of non-extractable C-14 residues suggesting that metabolites could be irreversibly sorbed, and (iii) an increase of K_d with time suggesting that IPU could be irreversibly sorbed. The



Fig. 4. Photo of the soil structure at the bottom of column I.

comparison of mass recovery rates between IPU and Met showed a higher leaching of Met in column I, while it showed contrasting results for column II with a higher leaching of Met at q_{\max} but a lower leaching of Met at q_{mid} . Except for the latter case, these results are in good agreement with the literature data (Agritox, 2001) on these two herbicides that suggests a higher mobility for Met than for IPU.

3.2. Numerical model analyses

Physical transport parameters were first estimated by inverting the Br BTCs for both columns using the CDE, MIM, DP and/or DP-MIM transport models. Then, chemical parameters for IPU and Met were estimated by inverting the herbicide BTCs using the physical transport model that best described Br transport combined with equilibrium or non-equilibrium chemical transport models. Note that non-equilibrium chemical transport is currently not yet available in the HYDRUS-1D model for the physical non-equilibrium DP-MIM transport model. The soil profile was assumed to be initially solute free. A prescribed solute flux (third-type boundary condition) and a zero concentration gradient were used as the upper and lower boundary conditions, respectively. Various models were calibrated against measured BTCs using flux concentrations at the lower boundary. For all simulations, the average pore water velocity, $v=q/\theta$, was fixed.

3.2.1. Physical transport parameters (analyses of the Br BTCs)

Results obtained by parameter optimization are presented in Fig. 1 and Table 2. The molecular diffusion coefficient of Br was taken as $0.066 \text{ cm}^2 \text{ h}^{-1}$ (Weast, 1985). The following physical transport parameters were fitted for different models: D and R for CDE; the dispersivity λ_m of the mobile phase (L), θ_{im} , and α_{ph} for MIM; q_{ma} , λ_f , w_f , and D_a for DP, and q_{ma} , λ_{ma} , λ_f , w_f , $q_{\text{im,ma}}$, D_a , and α_{ma} for DP-MIM. The following physical transport parameters were calculated from the fitted ones: the dispersivity $\lambda=D/v$ (L) for CDE; $\theta_m=\theta-\theta_{\text{im}}$ and the pore water velocity in the mobile phase $v_m=v\theta/\theta_m$ (LT^{-1}) for MIM; the contribution to the overall water content from the fracture and matrix domains

$\theta_f^* = w_f \theta_f$ and $\theta_{ma}^* = (1 - w_f) \theta_{ma}$, respectively, α_s calculated from Eq. (12), $q_f = (q - (1 - w_f) q_{ma}) / w_f$, pore water velocities in the fracture and matrix domain $v_f = q_f / \theta_f$ and $v_{ma} = q_{ma} / \theta_{ma}$, respectively, and the relative contribution of the fracture and matrix domain to the total flux $Q_f = w_f q_f / q$ and $Q_{ma} = (1 - w_f) q_{ma} / q$, respectively, for DP and DP-MIM; and additionally, $\theta_{m,ma}$ and the pore water velocity of the mobile domain of the matrix $v_{m,ma} = q_{ma} / \theta_{m,ma}$ (LT^{-1}) for DP-MIM. Note that for DP, the dispersivity in the matrix domain, λ_{ma} , was fixed. Fitting this parameter resulted in dramatically high confidence intervals for λ_{ma} and q_{ma} , suggesting that these parameters were not very sensitive due to the fact that the contribution of the matrix to the transport was rather small. Thus, we selected to fix λ_{ma} at a value of 1 cm, which is the commonly observed value for homogeneous soil columns (e.g., van Genuchten and Wierenga, 1977).

3.2.1.1. Physical equilibrium transport model — CDE. The CDE model did not describe satisfactorily the Br data for either column. Dispersivity values were significantly larger than the column length (q_{max} cases) or the retardation factors were larger than 1. In the CDE concept, solutes are transported through the entire pore space and CDE can not describe two arrival fronts as observed for both columns at q_{max} . Thus, large dispersivities accounted for physical non-equilibrium processes not considered in the CDE model, while retardation factors larger than 1 suggested that the CDE model used the sorption process to describe a potential storage of Br in immobile or low flow regions.

Only at q_{mid} , a good fit was obtained for column I but with a retardation factor significantly smaller than 1 ($R=0.76$). Such low R value could not be explained by anion exclusion alone. Considering a mean clay surface area of $130 \text{ m}^2 \text{ g}^{-1}$ (Bower and Hatcher, 1966) and an average double layer thickness of 5 Å (El-Swaify et al., 1967; Veeh et al., 1994), an exclusion volume of $0.04 \text{ cm}^3 \text{ g}^{-1}$ of clay was calculated. The total exclusion volume for the grassed soil column amounted thus only to about 3% of the total pore volume of the column. The low R value suggested an acceleration of the solute transport due to physical non-equilibrium processes.

From these results, it was concluded that the CDE transport model was not successful in modeling the bromide data for both columns and at all rainfall intensities.

3.2.1.2. Physical non-equilibrium transport model — MIM. The MIM model could not describe two arrival fronts in both columns at q_{max} (Fig. 1a and d). This result was expected since the MIM model can predict only one front since it has only one mobile zone.

For column I, at q_{mid} an excellent correspondence between the MIM model and data was obtained (Fig. 1b) with an immobile water content of $0.122 \text{ cm}^3 \text{ cm}^{-3}$. The mass transfer rate coefficient between mobile and immobile zones, α_{ph} , corresponded to a characteristic transfer time $t_{ph} = 1/\alpha_{ph} \sim 909 \text{ h}$, which is much longer than the bromide residence time, $t_r = LR/v \sim 79 \text{ h}$. This high value of t_{ph} suggested that not enough time was left for Br to diffuse into the microporosity during the experiment and that the mass transfer rate could be neglected at this time scale ($\alpha_{ph} \sim 0$), resulting thus in the symmetrical shape of the experimental BTC (van Genuchten and Wierenga, 1976). At q_{min} a good fit was found with an immobile water content of $0.245 \text{ cm}^3 \text{ cm}^{-3}$ and $t_{ph} = 81 \text{ h}$ compared to $t_r = 160 \text{ h}$ (Fig. 1c).

Table 2

Estimated physical transport parameters using four different physical transport models: the CDE, MIM, DP, and DP-MIM (for the highest velocity experiment only) transport models

		CDE						
		q cm h ⁻¹	λ cm	R –			r^2 –	
Column I	q_{\max}	0.308 (0.0162)	119.01 (27.50)	1.00 (349.80)			0.8371	
	q_{mid}	0.147 (0.0589)	8.17 (0.47)	0.76 (0.01)			0.9869	
	q_{\min}	0.0704 (0.01781)	14.69 (0.83)	1.10 (0.26)			0.8704	
Column II	q_{\max}	0.326 (0.0072)	69.94 (5.95)	1.00 (380.54)			0.8704	
	q_{mid}	0.1605 (0.0027)	28.00 (2.10)	1.20 (0.22)			0.9697	
		MIM						
		q cm h ⁻¹	λ_m cm	θ_m^a cm ³ /cm ⁻³	θ_{im} cm ³ /cm ⁻³	α_{ph} h ⁻¹	v_m^a cm h ⁻¹	r^2 –
Column I	q_{\max}	0.308 (0.0162)	4.13 (1.33)	0.088 (0.030)	0.310 (0.009)	0.0200 (0.0006)	3.517 (1.780)	0.9422
	q_{mid}	0.147 (0.0589)	5.48 (0.39)	0.264 (0.033)	0.122 (0.005)	0.0011 (0.0002)	0.557 (0.372)	0.9937
	q_{\min}	0.0704 (0.01781)	4.94 (0.61)	0.132 (0.016)	0.245 (0.008)	0.0123 (0.0013)	0.533 (0.225)	0.9880
Column II	q_{\max}	0.326 (0.0072)	43.78 (25.23)	0.238 (0.087)	0.136 (0.079)	0.0445 (0.0138)	1.368 (0.586)	0.9814
	q_{mid}	0.1605 (0.0027)	10.28 (2.58)	0.174 (0.035)	0.201 (0.026)	0.0266 (0.0098)	0.923 (0.246)	0.9876

		DP										
		q	λ_{ma}^b	λ_f	$\theta_{ma}^+{}^a$	$\theta_f^+{}^a$	$\alpha_s v_{ma}$	v_{ma}^a	v_f^a	Q_{ma}^a	Q_f^a	r^2
		cm h ⁻¹	cm	cm	cm ³ /cm ⁻³	cm ³ /cm ⁻³	h ⁻¹	cm h ⁻¹	cm h ⁻¹	–	–	–
Column I	q_{max}	0.308 (0.0162)	1.00	5.74 (1.58)	0.316 (0.033)	0.082 (0.012)	0.0443 (0.0150)	0.156 (0.076)	3.150 (1.189)	0.1597 (0.1339)	0.8403 (0.7045)	0.9408
	q_{mid}	0.147 (0.0589)	1.00	5.40 (0.36)	0.140 (0.065)	0.247 (0.037)	0.0059 (0.0015)	0.051 (0.059)	0.567 (0.474)	0.0482 (0.0813)	0.9518 (1.6049)	0.9935
	q_{min}	0.0704 (0.01781)	1.00	12.03 (4.22)	0.205 (0.037)	0.171 (0.028)	0.0212 (0.0015)	0.106 (0.034)	2.284 (0.302)	0.3078 (0.7274)	0.6922 (1.6360)	0.9881
Column II	q_{max}	0.326 (0.0072)	1.00	20.85 (6.98)	0.219 (0.048)	0.156 (0.040)	0.1829 (0.0600)	0.001 (0.128)	2.094 (1.023)	0.0004 (0.0005)	0.9996 (1.4104)	0.9785
	q_{mid}	0.1605 (0.0027)	1.00	11.18 (14.10)	0.197 (0.067)	0.178 (0.058)	0.1263 (0.1500)	0.027 (0.473)	0.872 (0.793)	0.0330 (0.1538)	0.9670 (4.5081)	0.9878

		DP-MIM														
		q	λ_{ma}	λ_f	$\theta_{ma}^+{}^a$	$\theta_f^+{}^a$	α_{-s}	$\theta_{m,ma}^a$	$\theta_{i,m,ma}$	α_{ma}	v_{ma}^a	v_f^a	$v_{m,ma}^a$	Q_{ma}^a	Q_f^a	r^2
		cm h ⁻¹	cm	cm	cm ³ cm ⁻³	cm ³ cm ⁻³	h ⁻¹	cm ³ cm ⁻³	cm ³ cm ⁻³	h ⁻¹	cm h ⁻¹	cm h ⁻¹	cm h ⁻¹	–	–	–
Column I	q_{max}	0.308 (0.0162)	0.16 (0.13)	0.03 (2.41)	0.39 (0.023)	0.002 (0.002)	0.0030 (0.0150)	0.063 (0.025)	0.334 (0.002)	0.0196 (0.0006)	0.715 (0.054)	16.043 (397.499)	4.519 (117.961)	0.9205 (47.3264)	0.0795 (4.0865)	0.9551
Column II	q_{max}	0.326 (0.0072)	8.30 (12.64)	7.84 (7.87)	0.347 (0.084)	0.027 (0.077)	0.0180 (0.1200)	0.223 (0.199)	0.124 (0.115)	0.0062 (0.0077)	0.590 (0.719)	4.475 (67.535)	0.918 (17.226)	0.6283 (22.4665)	0.3717 (13.2911)	0.9878

Standard errors are given in parenthesis, r^2 is the coefficient of determination for the regression of observed versus fitted concentrations, v_m , v_{ma} , v_f and $v_{m,ma}$ are average pore velocities in the mobile region of the MIM model, in matrix and fracture domain of the DP model, and in the mobile region of the matrix domain of the DP-MIM model, respectively, and Q_{ma} and Q_f are the relative contributions of the matrix and fracture region to the total flux, respectively.

^a Parameters calculated from the fitted parameters.

^b Fixed parameters.

For column II, at q_{mid} , the MIM model overestimated the experimental data, probably due to the low mass recovery of Br (83.3%) (Fig. 1e). The immobile water content was $0.201 \text{ cm}^3 \text{ cm}^{-3}$ and $t_{\text{ph}} = 38 \text{ h}$ compared to $t_r = 70 \text{ h}$.

Different transport mechanisms were thus found for the two columns, as already different shapes of the experimental BTCs suggested. For column I, a larger immobile domain for q_{min} compared to q_{mid} suggested that decreasing the velocity and the total water content created isolated zones in the soil that acted as immobile zones for the water flux (van Genuchten and Wierenga, 1977; Gaudet et al., 1977). At the q_{mid} case, a higher value of α_{ph} was found in column II compared to column I. This higher value is in agreement with the longer elution tail of the experimental BTC of column II compared to column I. Complex transport processes that depended on water flux (differences within a column) and on spatial variability (differences between columns) thus occurred in our two columns. It was concluded that the MIM model correctly simulates bromide transport at the intermediate and low rainfall intensities, although no explanation was found for the much lower value of α_{ph} at the intermediate rainfall intensity for column I. The MIM model was not well suited to model rapid preferential flow with two arrival fronts occurring at the largest rainfall intensities.

3.2.1.3. Physical non-equilibrium transport model — DP. For both columns, no significant differences were found between the optimized BTCs produced by the MIM and DP models. For all cases, the pore water velocities in the fracture domain were significantly higher than in the matrix domain. The relative contribution of the matrix domain to the total flux, Q_{ma} , differed between columns and flow rates. It was 15.97%, 4.82% and 30.78% for q_{max} , q_{mid} and q_{min} cases of column I and 0.04% and 3.33% for q_{max} and q_{mid} cases of column II. Thus, non-negligible contributions of the matrix domain were found for the q_{max} and q_{min} cases of column I. Note that large standard errors of estimated flux v_{ma} were obtained, compared to their mean values, when the contribution of the matrix domain to flow was negligible. Except for the q_{max} case of column II, the water content in the matrix domain was similar to the water content in the immobile domain found with the MIM model. Higher values of the mass transfer rate coefficient, α_s , between the fracture and matrix domains were found compared to α_{ph} of the MIM model (Table 2).

In general the dual-permeability model should be able to predict a double front solute migration when the transfer rate between the two domains is not too fast. However, in our case, the DP model, similarly to the MIM model, was not able to describe two arrival fronts that occurred during the Br transport at the highest rainfall intensities. Results found with MIM and DP models were quite similar since instead of an immobile zone considered in the MIM model, the DP model predicted very slow water flow in the matrix zone. This slow flow, together with higher fitted transfer rates, resulted into a single solute front predicted by the DP model. The effect of the slow flow zone would be more pronounced at smaller water fluxes than those used in our study.

3.2.1.4. Physical non-equilibrium transport model — DP-MIM. The dual-permeability mobile-immobile model was used to describe the transport of Br at the highest velocities. This model can well describe a double front solute migration due to faster flow in the

fracture domain and slower flow in the mobile zone of the matrix domain. While both MIM and DP models could relatively well describe the arrival of the main part of Br as well as the long tailing, they could not predict its very early arrival (time between 2 (0.05) and 6 (0.15) h (pore volume)). This could be achieved with the DP-MIM model, which added additional flexibility by providing additional pore region, i.e., fracture domain, through which Br could travel quickly, by-passing the matrix region and arriving early at the end of the column.

For column I, the DP-MIM model succeeded in describing the early solute front arrival, although the tail of the BTC was slightly overestimated, similarly as with the other transport models. For column II, the DP-MIM model was able to simulate well two solute peaks. Differences in pore velocities and water content in the fracture domain (Table 2) explained rather well observed differences between two experimental BTCs. For column I, the fastest zone (fracture domain) consisted of a very small pore domain ($\theta_f^* = 0.002 \text{ cm}^3 \text{ cm}^{-3}$ only) combined with a large pore velocity ($v_f = 16.043 \text{ cm h}^{-1}$). This resulted in the early front arrival of low concentrations after about 2 h of infiltration (0.05 pore volume), which corresponds with the time needed to travel through the 30-cm long column. The second large front was due to the matrix domain with a mobile water content, $\theta_{m,ma}$, equal to $0.063 \text{ cm}^3 \text{ cm}^{-3}$ and a pore velocity, $v_{m,ma}$, equal to 4.519 cm h^{-1} . For column II, the fastest zone (fracture domain) consisted of a larger, although still small, pore domain ($\theta_f^* = 0.027 \text{ cm}^3 \text{ cm}^{-3}$) combined with a smaller pore velocity ($v_f = 4.475 \text{ cm h}^{-1}$). This combination of the water content and pore velocity led to the arrival of the first peak of higher concentrations after about 8 h (0.23 pore volume), which is close to the time needed to travel through the 30-cm long soil column.

Different results were found for two mass transfer rate coefficients (α_s and α_{ma}) in the two columns. The mass transfer rate in column I was negligible between the fracture and matrix domains, and dominant between mobile and immobile regions of the matrix domain. Opposite results were found for column II (Table 2). These mass transfer rates reflect the shape of the BTCs in the two columns that also appeared very different (Fig. 1a and d). The BTC for column I shows two solute fronts of very different concentrations. The pore velocity in the fracture domain is very high and the mass transfer rate between fracture and matrix domains is small. The long concentration tail is then explained by large exchange between mobile and immobile regions of the matrix domain. The BTC for column II, on the other side, shows two solute peaks of similar magnitude and relatively smooth increases and decreases in concentrations, which requires faster exchange between the fracture and matrix domains. The latter mass transfer rate can explain the slight retardation observed between the measured arrival time of the first peak (about 8 h (0.23 pore volume)) and the arrival time calculated from v_f (6.7 h (0.19 pore volume)). Note that pore velocities in the fracture domain of column II are of similar magnitude as pore velocities in the mobile region of the matrix domain of column I, and so are the mass transfer rate coefficients between these and slower, or stagnant, regions.

Relative contributions of the matrix domain to the total flow was 92.05% and 62.83% for columns I and II, respectively. Although larger pores (fracture domain) are responsible for an early arrival of the solute, they do not contribute a large part of the total flux. Large macropores generally account for the main part of the flow rate at full saturation, but are inactive for unsaturated flow. Under experimental conditions in our study, macropores

were inactive for medium and low rainfall intensities, but became partly active for the highest fluxes. Their effect would start dominating flow if full saturation was reached.

3.2.1.5. Intermediate conclusions about bromide transport modeling. Physical non-equilibrium models of different types (MIM, DP, DP-MIM) better described bromide transport than physical equilibrium model (CDE). A preferential flow of a macropore type was suggested based on the experimental data for the highest rainfall intensities (two arrival fronts and marked shift to the left of peak positions). The DP-MIM model better modeled the experimental data than the other non-equilibrium transport models (MIM and DP) and supported the hypothesis of multiple (three) porosity domains with multiple (two) permeabilities at this rainfall intensity. However, an important note has to be made concerning the confidence one can have in these simulations. Non-negligible cross-correlations between a large number of parameters and non-unique solutions were found for both columns. These problems were already discussed by many authors (e.g., Brusseau et al., 1989; Hopmans et al., 2002). It must be kept in mind that the DP-MIM simulations made here must be considered as a working hypothesis for testing the concept of multiple porosities and permeabilities on our data rather than a definite answer. A preferential flow of a different type, close to a MIM type, was suggested for experiments at the other velocities. No significant differences were found in the fits given by the MIM and DP models, confirming therefore the hypothesis of a two-domain transport. However, in the case of the lowest rainfall intensity, the DP model showed that the contribution of the matrix to the total flux can be significant. From these results, it was concluded that at intermediate and low rainfall intensities, the preferential transport observed is of a dual porosity type with a zero or low flow in the matrix domain.

3.2.2. Chemical transport parameters (analyses of the herbicide BTCs)

Results of the model analyses of the herbicide BTCs are presented in Figs. 2 and 3 and Table 3. In the following analyses with chemical equilibrium and non-equilibrium models, the first-order degradation rate, μ_w , was estimated although no degradation products were detected. As mentioned, the fact that no degradation products were detected in the effluents did not mean that no decay processes occurred. The decay processes hypothesized in Section 3.1 were (i) degradation with the formation of metabolites of lower mobility than the parent compound, (ii) mineralization or (iii) irreversible sorption of either the parent compound or the metabolites. The models used in this study assumed a total mass recovery of the chemicals so that all processes responsible for the loss of solute and not included in the governing equations (degradation, mineralization, irreversible sorption) are lumped into the first-order degradation rate μ_w .

3.2.2.1. Chemical equilibrium transport model — (DP-MIM and DP)- K_d . The dual-permeability mobile-immobile model was used as the transport model for the highest velocity experiments, while the dual-permeability model was considered for the other velocities. The physical transport parameters (λ_{ma} , λ_f , θ_{ma}^* , θ_f^* , v_{ma} , and v_f for DP, and additionally $\theta_{m,ma}$, $\theta_{im,ma}$, and $v_{m,ma}$ for DP-MIM) were fixed to values estimated for the Br transport. The mass transfer rate coefficients for the chemicals (α_s for DP plus α_{ma} for DP-MIM) were calculated from the ones estimated for Br, corrected for the molecular

Table 3

Estimated chemical transport parameters for isoproturon and metribuzin using DP transport model combined with non-equilibrium chemical model (instantaneous and first-order kinetic retention) (DP-(K_d , α_{ch}) transport model)

		IPU							
		q	K_d	f_{ma}	f_f	α_{ch}	μ_w	DT50 ^a	r^2
		cm h ⁻¹	l kg ⁻¹	–	–	h ⁻¹	h ⁻¹	d	–
Column I	q_{max}	0.308 (0.0162)	1.31 (0.16)	0.131 (7.136)	0.115 (0.024)	0.0547 (0.0060)	0.0755 (0.0036)	0.38 (0.02)	0.9739
	q_{mid}	0.147 (0.0589)	1.70 (0.12)	0.991 (0.001)	0.219 (0.025)	0.0124 (0.0015)	0.0190 (0.006)	1.52 (0.05)	0.9341
	q_{min}	0.0704 (0.01781)	2.24 (0.39)	0.183 (1.319)	0.286 (0.049)	0.0067 (0.0376)	0.0178 (0.0166)	1.62 (1.51)	0.7454
Column II	q_{max}	0.326 (0.0072)	1.28 (0.07)	0.994 (0.000)	0.036 (0.008)	0.0746 (0.0040)	0.0107 (0.0019)	2.69 (0.47)	0.9824
	q_{mid}	0.1605 (0.0027)	1.50 (0.16)	0.117 (1.872)	0.003 (0.007)	0.0397 (0.0019)	0.0040 (0.0011)	7.26 (1.99)	0.9600
		Met							
		q	K_d	f_{ma}	f_f	α_{ch}	μ_w	DT50 ^a	r^2
		cm h ⁻¹	l kg ⁻¹	–	–	h ⁻¹	h ⁻¹	d	–
Column I	q_{max}	0.308 (0.0162)	1.17 (0.19)	0.137 (4.480)	0.082 (0.022)	0.0575 (0.0038)	0.0255 (0.0027)	1.29 (0.15)	0.9743
	q_{min}	0.0704 (0.01781)	0.73 (0.09)	0.161 (1.427)	0.289 (0.051)	0.0199 (0.0028)	0.0040 (0.005)	7.16 (0.80)	0.9705
Column II	q_{max}	0.326 (0.0072)	0.64 (0.10)	0.321 (2.863)	0.004 (0.014)	0.1296 (0.0189)	0.0065 (0.0020)	4.45 (1.35)	0.9799
	q_{mid}	0.1605 (0.0027)	0.68 (0.03)	0.000 (0.848)	0.015 (0.013)	0.0698 (0.0026)	0.0123 (0.0004)	2.36 (0.07)	0.9902

Standard errors are given in parenthesis and r^2 is the coefficient of determination for the regression of observed versus fitted concentrations.

^a Parameters calculated from the fitted parameters.

diffusion coefficient of pesticides, taken as 0.0179 cm² h⁻¹ (Jury et al., 1983). The number of chemical parameters to be estimated was therefore limited to K_d and μ_w for the DP model, and additionally $f_{m,ma}$ for the DP-MIM model.

Results showed that for all rainfall intensities and regardless of the used physical transport model the chemical equilibrium transport model was not well suited to describe the transport of herbicides in the grassed soil columns. Systematically, the model strongly underestimated the observed elution tails and could not correctly predict the arrival time of the first herbicide non-zero concentrations and peak positions (Figs. 2 and 3).

3.2.2.2. *Chemical non-equilibrium transport model — DP-(K_d , α_{ch})*. Chemical non-equilibrium is not currently available in the dual-permeability mobile-immobile transport model of HYDRUS-1D. Therefore, we used the dual-permeability model as the physical transport model also for the highest velocity cases in order to estimate the importance of non-equilibrium chemical transport for the two herbicides. The dual-permeability model was thus viewed as an approximation of the physical transport occurring at the highest

rainfall intensities. Similarly as for the chemical equilibrium model, the physical transport parameters (λ_{ma}^* , λ_{f}^* , θ_{ma}^* , θ_{f}^* , v_{ma} , v_{f}) were fixed to the values estimated for Br transport and the chemicals mass transfer rate coefficients (α_{s}) were calculated from the ones obtained for Br, corrected for the molecular diffusion coefficient of pesticides. The chemical parameters to estimate were therefore K_{d} , α_{ch} , f_{ma} , f_{f} and μ_{w} .

For both herbicides, the non-equilibrium chemical model described well the experimental BTCs. Particularly, the elution tails of BTCs were well captured. Only the early arrival of isoproturon for the q_{min} case of column I was not well described (Fig. 2c). The early arrival front at q_{max} for column I was not described (Figs. 2a and 3a).

A comparison of the sorption parameters (K_{d} and α_{ch}) between the two herbicides showed higher K_{d} values for IPU and comparable to higher α_{ch} values for Met (Table 3). A higher sorption capacity of the soil for IPU compared to Met is in agreement with the literature data that show that Met is more mobile than IPU (Agritox, 2001). The absolute K_{oc} values, calculated as $K_{\text{oc}} = K_{\text{d}} / \text{CO}$ with CO being the organic carbon content (equal to 17.29 g kg⁻¹ from Madrigal et al., 2002) were in the range of 74 to 130 l kg⁻¹ for IPU and 37 to 68 l kg⁻¹ for Met. These values were thus also in the range of the literature data (Agritox, 2001). For IPU, the K_{d} values were lower than those derived from batch sorption experiments with the same soil data (Madrigal et al., 2002). Note that good fits could not be found when the K_{d} parameter was fixed to the latter batch value of 2.4 l kg⁻¹.

For IPU, K_{d} values increased when rainfall intensities decreased, with comparable values between the two columns. For Met, no significant trend was observed for K_{d} values. For both herbicides, a significant decrease in the sorption kinetic rate coefficient, α_{ch} , was observed as velocity decreased. Maraqa (2001), in a review of column displacement experiments, reported similar trends. A possible explanation is that for lower velocities more sites seem to be at relative equilibrium with the solution (f_{f} usually increased when velocity decreased), and given the lower sorption kinetic rate the overall rate of reaction is then more or less the same. Note that the values of f_{ma} were all accompanied by very large errors or were found to be close to 1. A series of additional simulations was performed with this parameter fixed to different values (0.1, 0.5 and 0.9). No significant differences were found in simulated BTCs, showing that f_{ma} is not a sensitive parameter for the herbicide transport. Since the flow in the matrix region is slower, there is more time to reach equilibrium in the matrix domain and thus the fraction of exchange sites assumed to be in equilibrium with the solution phase of the matrix domain is not a relevant parameter. Equilibrium sorption in the matrix domain is thus a suitable model. By contrast, for the fracture domain where there is not enough time to reach equilibrium, due to faster flow, non-equilibrium sorption is an appropriate model to explain the observed long elution tails. Sensitivity analyses performed with f_{f} fixed to different values (0.1, 0.5 and 0.9) showed that the elution tails can not be described with large f_{f} values (0.5 and 0.9).

Using soil samples originating from the same grassed strip, Benoit et al. (1999) have shown an increase in IPU sorption during soil incubation at 18 °C and the water content close to the soil water holding capacity. This was done by considering extractions with calcium chloride and methanol at different dates and soil depths (0–2; 2–13 and 13–30 cm) where the herbicide concentration was measured by HPLC. From these data, we estimated a mean sorption kinetic rate parameter for IPU using a simple first order equation to fit the increase in sorbed IPU versus time and considering the 0–30 cm horizon as one single

layer. We calculated a value of 0.0122 h^{-1} which is of the same order of magnitude as the IPU α_{ch} values estimated by the DP- $(K_{\text{d}}, \alpha_{\text{ch}})$ model (Table 3).

A longer half-life for IPU compared to Met for q_{mid} case of column II and lower DT50s for all other cases are in agreement with the IPU mass recovery rates in the effluent that are higher for q_{mid} case of column II and smaller for all other cases compared to Met (Table 1). However, the DT50s values were dramatically lower than the lower bounds of the literature ranges for both pesticides. Fitted degradation rates were up to 31 and 18 times larger for IPU and Met, respectively, than the literature values (Agritox, 2001). Although attempts have been made to fit IPU BTCs with μ_{w} fixed to the measured batch value of 0.001203 h^{-1} in the grassed strip soil (Benoit et al., 1999), no good fits could be found.

Several other authors have also found markedly faster degradation rates in column displacement studies compared to batch data. Up to 3 times larger degradation rates for saturated experiments and up to 14 times for unsaturated experiments were found by Rocio Estrella et al. (1993); and up to 7 times larger rates in saturated experiments were found by Guo and Wagenet (1999). Other authors found higher or comparable degradation rates (Gaston et al., 2003; Das et al., 2004) and/or smaller degradation rates (Langner et al., 1998; Simoni et al., 2001). Higher degradation rates in column displacement experiments compared to batch data were usually attributed to differences in aeration and mixing in the batch and column systems, to decrease of substrate concentrations in batch experiments compared with constant influent substrate concentrations in column experiments, or to a high degree of non-equilibrium sorption (Guo and Wagenet, 1999). Smaller degradation rates were attributed to rate-limited diffusion of the solutes to the microbial cells (Simoni et al., 2001).

The first-order degradation rate, μ_{w} , was found to increase when velocity increased, except for Met of column II. Anglely et al. (1992) and Guo and Wagenet (1999) found similar results for alkylbenzenes and alachlor, respectively. Our modeling analysis suggested that the degree of non-equilibrium sorption increased as velocity increased (f_{f} usually decreased). Thus, our results suggest that the estimated degradation rates are positively related to the degree of non-equilibrium sorption. It supports the hypothesis that chemical irreversible sorption, defined as fast attachment and much slower detachment, occurred most probably on the sorption sites where kinetic sorption occurs. The irreversible sorption acts as a disappearance process at the time scale of our experiments and is therefore accounted for by apparently higher degradation rates by the models. This could explain the apparent contradiction of higher degradation rates when higher mass recovery rates in the effluent are measured.

4. Conclusions

Two series of Br and herbicides (IPU and Met) displacement experiments were performed at different rainfall intensities (0.070, 0.147, 0.161, 0.308 and 0.326 cm h^{-1}) in two soil columns sampled in a 10-year-old grassed strip at La Jaillièrè. The experimental Br BTCs, and their descriptive and numerical analyses, suggested two contrasted physical non-equilibrium processes depending on the rainfall intensity. For the highest rainfall intensities (0.308 and 0.326 cm h^{-1}), multiple porosity domains and multiple

permeabilities preferential flow were probably active: a) rapid flow through macropore pathways, b) slower flow through a mesoporosity, and c) no-flow in the remaining micropores. The total mobile porosity was suggested to be less than $0.07 \text{ cm}^3 \text{ cm}^{-3}$ in terms of the water content. For the lower rainfall intensities, macropore flow was not active anymore.

The experimental BTCs of both herbicides confirmed the hypothesis of a rapid preferential flow at the highest rainfall intensities. The main conclusion drawn from the modeling analyses is that non-equilibrium chemical transport processes occurred for all velocities and both herbicides and that the degree of non-equilibrium sorption increased with velocity. IPU was found less mobile than Met in accordance with batch data. Significantly higher values of degradation rate parameters as compared to batch data were positively related with the degree of non-equilibrium sorption. This work suggests that the sorption and/or degradation rates obtained from batch experiments can not be used in non-equilibrium transport models to describe the transport experiments unless the actual underlying mechanisms measured by the two techniques are fully identified.

From an environmental point of view, these series of displacement experiments allowed to better understand the functioning of the grassed strip at La Jaillière. Particularly, these results emphasized the potential role of macropores in establishing rapid preferential transport of herbicides and in by-passing the surface layer of the grassed soil at a relatively low rainfall intensity (0.3 cm h^{-1}). This work should be completed with displacement experiments under ponding conditions, as the grassed strip soils are mainly used as protective management practices for the reduction of pesticides from agricultural runoff waters.

Acknowledgments

We would like to thank Christophe Labat for his help in sampling at the experimental site. This study was supported financially by the INRA-Cemagref “AQUAE” program and the Pesticide Research program of the French Ministry of the Ecology and Sustainable Development. Support from OECD (a fellowship under the OECD Co-operative Research Program: Biological Resource Management for Sustainable Agriculture Systems) and INRA for J. Šimůnek’s summer stay at the UMR INRA/INAPG EGC-Grignon is greatly acknowledged.

References

- Agritox: Toxological Data Base on Pesticides, 2001. INRA, France.
- Angley, J.T., Brusseau, M.L., Lamar Miller, W., Delfino, J.J., 1992. Nonequilibrium sorption and aerobic biodegradation of dissolved alkybenzenes during transport in aquifer material: column experiments and evaluation of a coupled-process model. *Environ. Sci. Technol.* 26, 1404–1410.
- Arora, K., Mickelson, S.K., Baker, J.L., Tierney, J.L., Peters, C.J., 1996. Herbicide retention by vegetative buffer from runoff under natural rainfall. *Trans. ASAE* 39, 2155–2162.
- Baker, J.L., Mickelson, S.K., Hatfield, J.L., Fawcett, R.S., Hoffman, D.W., Franti, T.G., Tierney, D.P., 1995. Reducing herbicide runoff: role of best management practices. In *British Crop Prot. Conf. — Weeds*. BCPC Publications, Farnham, pp. 479–487.

- Benoit, P., Barriuso, E., Vidon, P., Réal, B., 1999. Isoproturon sorption and degradation in a soil from grassed buffer strip. *J. Environ. Qual.* 28, 121–129.
- Benoit, P., Barriuso, E., Vidon, P., Réal, B., 2000. Isoproturon movement and dissipation in undisturbed soil cores from a grassed buffer strip. *Agronomie* 20, 297–307.
- Bower, C.A., Hatcher, J.T., 1966. Simultaneous determination of surface area and cation-exchange capacity. *Soil Sci. Soc. Am. Proc.* 30, 525–527.
- Brusseau, M.L., Jessup, R.E., Rao, P.S.C., 1989. Modeling the transport of solutes influenced by multiprocess nonequilibrium. *Water Resour. Res.* 25, 1971–1988.
- Cameron, D.R., Klute, A., 1977. Convective–dispersive solute transport with a combined equilibrium and kinetic adsorption model. *Water Resour. Res.* 13, 183–188.
- Das, B.S., Lee, L.S., Rao, P.S.C., Hultgren, R.P., 2004. Sorption and degradation of steroid hormones in soils during transport: column studies and model evaluation. *Environ. Sci. Technol.* 38, 1460–1470.
- Delphin, J.-E., Chapot, J.-Y., 2001. Leaching of atrazine and deethylatrazine under a vegetative filter strip. *Agronomie* 21, 461–470.
- Dillaha, T.A., Reneau, R.B., Mostaghimi, S., Lee, D., 1989. Vegetative filter strips for agricultural nonpoint source pollution control. *Trans. ASAE* 32, 513–519.
- El-Swaify, S., Coleman, N.T., Bredell, G., Arca, M., 1967. Negative adsorption by vermiculite: salt exclusion from interlayer volumes. *Soil Sci. Soc. Am. Proc.* 31, 464–466.
- Gaston, L.A., Boquet, D.J., Bosch, M.A., 2003. Fluometuron sorption and degradation in cores of silt loam from different tillage and cover crop systems. *Soil Sci. Soc. Am. J.* 67, 747–755.
- Gaudet, J.-P., Jégat, H., Vachaud, G., Wierenga, P.J., 1977. Solute transfer, with exchange between mobile and stagnant water, through unsaturated sand. *Soil Sci. Soc. Am. J.* 41, 665–671.
- Gerke, H.H., van Genuchten, M.Th., 1993. A dual-porosity model for simulating the preferential movement of water and solutes in structured porous media. *Water Resour. Res.* 29, 305–319.
- Gerke, H.H., van Genuchten, M.Th., 1996. Macroscopic representation of structural geometry for simulating water and solute movement in dual-porosity porous media. *Adv. Water Resour.* 19, 343–357.
- Guo, L., Wagenet, R.J., 1999. Evaluation of alachlor degradation under transport conditions. *Soil Sci. Soc. Am. J.* 63, 443–449.
- Haynes, R.J., Francis, G.S., 1993. Changes in microbial biomass C, soil carbohydrate composition and aggregate stability induced by growth of selected crop and forage species under field conditions. *J. Soil Sci.* 44, 665–675.
- Hopmans, J.W., Šimůnek, J., Romano, N., Durner, W., 2002. Inverse modeling of transient water flow. In: Dane, J.H., Topp, G.C. (Eds.), *Methods of Soil Analysis: Part 1. Physical Methods*, Chapter 3.6.2, Third edition. SSSA, Madison, WI, pp. 963–1008.
- Hurto, K.A., Turgeon, A.J., Cole, M.A., 1979. Degradation of benefin and DCPA in thatch and soil from Kentucky Bluegrass (*Poa pratensis*) turf. *Weed Sci.* 27, 154–157.
- Jury, W.A., Spencer, W.F., Farmer, W.J., 1983. Behavior assessment model for trace organics in soil: I. Model description. *J. Environ. Qual.* 12, 558–564.
- Kanchanasut, P., Scotter, D.R., 1982. Leaching patterns in soil under pasture and crop. *Aust. J. Soil Res.* 20, 193–202.
- Kay, B.D., 1990. Rates of changes of soil structure under different cropping systems. In: Steward, B.A. (Ed.), *Advances in Soil Science*. Springer-Verlag, pp. 1–51.
- Langner, H.W., Inskip, W.P., Gaber, H.M., Jones, W.L., Das, B.S., Wraith, J.M., 1998. Pore water velocity and residence time effects on the degradation of 2,4-D during transport. *Environ. Sci. Technol.* 32, 1308–1315.
- Lapidus, L., Amundson, N.R., 1952. Mathematics of adsorption in beds: VI. The effect of longitudinal diffusion in ion exchange and chromatographic columns. *J. Phys. Chem.* 56, 84–988.
- Madrigal, I., Benoit, P., Barriuso, E., Etiévant, V., Souiller, C., Réal, B., Dutertre, A., 2002. Capacités de stockage et d'épuration des sols de dispositifs enherbés vis-à-vis des produits phytosanitaires. Deuxième partie: propriétés de rétention de deux herbicides, l'isoproturon et le diflufenicanil dans différents sols de bandes enherbées. *Etude et Gestion des Sols* 9, 287–302.
- Maraqa, M.A., 2001. Prediction of mass-transfer coefficient for solute transport in porous media. *J. Contam. Hydrol.* 50, 1–19.

- Merckx, R., Den Hartog, A., Van Veen, J.A., 1985. Turnover of root-derived material and related biomass formation in soils of different texture. *Soil Biol. Biochem.* 17, 565–569.
- Mersie, W., Seybold, C., Tsegaye, T., 1999. Movement, adsorption and mineralization of atrazine in two soils with and without switchgrass (*Panicum virgatum*) roots. *Eur. J. Soil Sci.* 50, 343–349.
- Patty L., 1997. Limitation du transfert par ruissellement vers les eaux superficielles de deux herbicides (isoproturon et diflufenicanil). Méthodologie analytique et étude de l'efficacité de bandes enherbées. PhD Thesis. Université Joseph Fourier, Grenoble, France.
- Patty, L., Réal, B., Gril, J.-J., 1997. The use of grassed buffer strips to remove pesticides, nitrate and soluble phosphorus compounds from runoff water. *Pest. Sci.* 49, 243–251.
- Reungsang, A., Moorman, T.B., Kanwar, R.S., 2001. Transport and fate of atrazine in midwestern riparian buffer strips. *J. Am. Water Resour. Assoc.* 37, 1681–1692.
- Rocio Estrella, M., Brusseau, M.L., Maier, R.S., Pepper, I.L., Wierenga, P.J., Miller, R.M., 1993. Biodegradation, sorption, and transport of 2,4-Dichlorophenoxyacetic acid in saturated and unsaturated soils. *Appl. Environ. Microbiol.* 59, 4266–4273.
- Selim, H.M., Davidson, J.M., Rao, P.S.C., 1977. Transport of reactive solutes through multilayered soils. *Soil. Sci. Soc. Am. J.* 41, 3–10.
- Simoni, S.F., Schäfer, A., Harms, H., Zehnder, A.J.B., 2001. Factors affecting mass transfer limited biodegradation in saturated porous media. *J. Contam. Hydrol.* 50, 99–120.
- Šimůnek, J., Šejna, M., van Genuchten, M.Th., 1998. The HYDRUS-1D software package for simulating the one-dimensional movement of water, heat, and multiple solutes in variably-saturated media. Version 2.0, *IGWMC-TPS-70*. International Ground Water Modeling Center, Colorado School of Mines, Golden, Colorado. 202 pp.
- Šimůnek, J., Wendroth, O., Wypler, N., van Genuchten, M.Th., 2001. Nonequilibrium water flow characterized from an upward infiltration experiment. *Eur. J. Soil Sci.* 52 (1), 13–24.
- Šimůnek, J., Jarvis, N.J., van Genuchten, M.Th., Gärdenäs, A., 2003. Review and comparison of models for describing non-equilibrium and preferential flow and transport in the vadose zone. *J. Hydrol.* 272, 14–35.
- Souiller, C., Coquet, Y., Pot, V., Benoit, P., Réal, B., Margoum, C., Laillet, B., Labat, C., Vachier, P., Dutertre, A., 2002. Capacités de stockage et d'épuration des sols de dispositifs enherbés via-à-vis des produits phytosanitaires. Première partie: dissipation des produits phytosanitaires à travers un dispositif enherbé; mise en évidence des processus mis en jeu par simulation de ruissellement et infiltrométrie. *Etude et Gestion des Sols* 9, 269–285.
- van Genuchten, M.Th., Wierenga, P.J., 1976. Mass transfer studies in sorbing porous media I. Analytical solutions. *Soil Sci. Soc. Am. J.* 40, 473–480.
- van Genuchten, M.Th., Wierenga, P.J., 1977. Mass transfer studies in sorbing porous media II. Experimental evaluation with tritium ($^3\text{H}_2\text{O}$). *Soil Sci. Soc. Am. J.* 41, 272–278.
- van Genuchten, M.Th., Wagenet, R.J., 1989. Two-site/two-region models for pesticide transport and degradation: theoretical development and analytical solutions. *Soil Sci. Soc. Am. J.* 53, 1303–1310.
- Veeh, R.H., Inskeep, W.P., Roe, F.L., Ferguson, A.H., 1994. Transport of chlorsulfuron through soil columns. *J. Environ. Qual.* 23, 542–549.
- Vogeler, I., Scotter, D.R., Green, S.R., Clothier, B.E., 1997. Solute movement through undisturbed soil columns under pasture during unsaturated flow. *Aust. J. Soil Res.* 35, 1153–1163.
- Weast, R.C., 1985. *Handbook of Chemistry and Physics*, 66th edition. CRC Press, Boca Raton, Florida.